Published in final edited form as:
J Mol Cell Cardiol. 2008 December ; 45(6): 715–723. doi:10.1016/j.yjmcc.2008.08.015.

Histone-deacetylase Inhibition Reverses Atrial Arrhythmia Inducibility and Fibrosis in Cardiac Hypertrophy Independent of Angiotensin

Fang Liu, PhD[1], **Mark D. Levin, MD**[1,2], **Nataliya B. Petrenko, MS**[1], **Min Min Lu, MD**[1], **Tao Wang, MD, PhD**[1], **Li Jun Yuan, MD**, **Andrea L. Stout, PhD**[3], **Jonathan A. Epstein, MD**[1,2,3], and **Vickas V. Patel, MD, PhD**[1]

1*Penn Cardiovascular Institute, University of Pennsylvania, Philadelphia, PA*

2*Division of Cardiology, Department of Pediatrics, Children's Hospital of Philadelphia, Philadelphia PA*

3*Department of Cell and Developmental Biology, University of Pennsylvania, Philadelphia, PA*

Abstract

Atrial fibrosis influences the development of atrial fibrillation (AF), particularly in the setting of structural heart disease where angiotensin-inhibition is partially effective for reducing atrial fibrosis and AF. Histone-deacetylase inhibition reduces cardiac hypertrophy and fibrosis, so we sought to determine if the HDAC inhibitor trichostatin A (TSA) could reduce atrial fibrosis and arrhythmias. Mice over-expressing homeodomain-only protein ($HopX^{Tg}$), which recruits HDAC activity to induce cardiac hypertrophy were investigated in 4 groups (aged 14-18 weeks): wild-type (WT), $HopX^{Tg}$, $HopX^{Tg}$ mice treated with TSA for 2 weeks (HopX-TSA) and wild-type mice treated with TSA for 2 weeks (WT-TSA). These groups were characterized using invasive electrophysiology, atrial fibrosis measurements, atrial connexin immunocytochemistry and myocardial angiotensin II measurements. Invasive electrophysiologic stimulation, using the same attempts in each group, induced more atrial arrhythmias in $HopX^{Tg}$ mice (48 episodes in 13 of 15 $HopX^{Tg}$ mice versus 5 episodes in 2 of 15 HopX-TSA mice, $P<0.001$; versus 9 episodes in 2 of 15 WT mice, $P<0.001$; versus no episodes in any WT-TSA mice, $P<0.001$). TSA reduced atrial arrhythmia duration in $HopX^{Tg}$ mice (1307±289 milliseconds versus 148±110 milliseconds, $P<0.01$) and atrial fibrosis (8.1 ±1.5% versus 3.9±0.4%, $P<0.001$). Atrial connexin40 was lower in $HopX^{Tg}$ compared to WT mice, and TSA normalized the expression and size distribution of connexin40 gap junctions. Myocardial angiotensin II levels were similar between WT and $HopX^{Tg}$ mice (76.3±26.0 versus 69.7±16.6 pg/mg protein, *P*=NS). Therefore, it appears HDAC inhibition reverses atrial fibrosis, connexin40 remodeling and atrial arrhythmia vulnerability independent of angiotensin II in cardiac hypertrophy.

Keywords

atrial arrhythmias; histone deacetylases; fibrosis; connexin40; heart failure

Address correspondence to: Vickas Patel, MD, PhD, 907 BRB II/III, 421 Curie Blvd., Philadelphia, PA 19104, Phone: (215) 898-2800; Fax: (215) 573-2094, E-mail: vickas.patel@uphs.upenn.edu.

1. Introduction

Atrial fibrillation (AF) is the most common clinical cardiac arrhythmia encountered and is highly prevalent in heart failure. In particular, left ventricular hypertrophy and diastolic dysfunction are independent risk factors for the development of AF [1,2]. Antiarrhythmic drug therapy has a relatively low efficacy for restoring and maintaining sinus rhythm. However, the discovery pulmonary vein triggers initiate AF has led to catheter-based techniques as a reliable therapy for this disease. Pulmonary vein isolation offers benefits over antiarrhythmic drugs, and is effective in patients with normal hearts, but present techniques are less effective in the setting of structural heart disease such as left ventricular hypertrophy [3].

Atrial electrical remodeling contributes to the perpetuation of AF, although it may also be a consequence of the arrhythmia. In this regard, evidence suggests atrial structural changes alone are sufficient to promote AF [4]. Angiotensin-inhibition affects myocardial remodeling and fibrosis through its action upon multiple pathways. These include transforming growth factor beta-1 (TGF-β1) signaling, and mitogen-activated protein kinases (MAPK). Experimental and clinical evidence support the ability of angiotensin-inhibition to reduce AF [5], however angiotensin-independent pathways also contribute to atrial structural remodeling and AF [6]. Therefore, elucidation of angiotensin-independent pathways that promote atrial structural remodeling may lead to novel therapies for AF in the setting of left ventricular hypertrophy.

In this report we present evidence histone-deacetylase inhibition (HDACi) reverses atrial fibrosis and arrhythmic inducibility in *HopX* transgenic mice with left ventricular hypertrophy. Cardiac hypertrophy induced by *HopX* over-expression is associated with atrial fibrosis and increased AF inducibility, but does not affect myocardial angiotensin II levels. Therefore, in this particular model HDACi reduces atrial arrhythmogenesis through favorable effects upon atrial structural remodeling independent of angiotensin.

2. Materials and methods

Key methodological components used are described below in abbreviated form. A full description of all methods is available in the online Data Supplement.

2.1 Animals

Creation of *HopX* transgenic mice ($HopX^{Tg}$) has been previously described [7]. Fourteen to eighteen week-old $HopX^{Tg}$ (TSA-$HopX^{Tg}$) and wild-type (TSA-WT) mice were administered 0.6 mg/kg/day Trichostatin A (TSA, Sigma-Aldrich) by intraperitoneal injection for 14 days; and compared to age-matched $HopX^{Tg}$ mice injected with saline for the same duration or wild-type littermates given no treatment. All protocols conformed to the guidelines established by the Association for the Assessment and Accreditation of Laboratory Animal Care and were approved by the University of Pennsylvania Animal Care and Use Committees. The investigation conforms to the *Guide for the Care and Use of Laboratory Animals* published by the US National Institutes of Health (NIH Publication No. 85-23, revised 1996).

2.2 In vivo electrophysiology

Four groups of animals, $HopX^{Tg}$, WT, TSA-WT (n=15) and TSA-HopX mice (n=10) were anesthetized with pentobarbital (33 mg/kg IP) and multi-lead ECGs obtained. An octapolar 1.7-French electrode catheter (CIBer mouse-EP; NuMED) was placed in the right atrium and ventricle under electrogram guidance through a jugular vein cutdown. A programmed digital stimulator (DTU-215, Fischer Scientific) delivered electrical impulses at ~twice diastolic threshold, while surface ECG and intracardiac electrograms were displayed on a multichannel oscilloscope recorder (Bard Electrophysiology, Inc.) and analyzed offline. We defined an

arrhythmic episode as induction of three or more consecutive ectopic beats following the last extrastimuli.

2.3 Invasive hemodynamics

Invasive hemodynamic recordings were obtained from the four groups of mice (n=7 in each group). Anesthesia was induced by ventilation with isoflurane. A microtip pressure–volume catheter (SPR-839; Millar Instruments) was advanced into the left ventricular via the right carotid artery to measure intracardiac pressures. Traces were digitized at 2-kHz using a PowerLab/16 SP A/D converter (ADInstruments Ltd.) and analyzed offline.

2.4 Echocardiography

Mice from the four different groups (n=7 in each group) were anesthetized using an integrated isoflurane-based system. Two-dimensional images were obtained at 180 frames/second using a 30-MHz probe (RMV 707B, Visual Sonics) in the parasternal long- and short-axis views to obtain left atrial dimensions and guide M-mode analysis at the mid-ventricular level. Pulsed doppler recordings were obtained in the apical four-chamber view from the mitral valve and pulmonary veins. LV fractional shortening, ejection fraction and wall dimensions were computed from M-mode measurements.

2.5 Histological analysis of fibrosis

Animals were euthanized using pentobarbital overdose and whole hearts immersed in 2% neutral buffered formalin for 24 hours (n=3 in each group). Fixed hearts were embedded in paraffin, sectioned (5μm) and stained with Masson's trichrome. For each section, non-overlapping photomicrographs (400x) were taken from the entire left atrium up to, but not including, the mitral annulus. Sections were analyzed using the ImageJ software (NIH) to compute fractional area of fibrosis (blue regions) as a percentage of total myocardial area.

2.6 Tissue angiotensin II assay

Whole hearts were isolated from $HopX^{Tg}$ and TSA-HopX mice (n=3 in each group) homogenized in acetic acid and cleared by centrifugation. Supernatants were purified on a C18 Sep-Pak column (Waters Associates) and eluted with acetonitrile and trifluoroacetic acid. Angiotensin II concentration was determined from paired samples, with equal amounts of protein, by ELISA using an anti–angiotensin II antibody (Peninsula ELISA) and biotinylated angiotensin II as a tracer.

2.7 Adult atrial myocyte isolation

Mice were heparizined (100 units IP), anesthetized with pentobarbital (50 mg/kg) and hearts excised through a sternotomy (n=3 in each group). Hearts were mounted on a Langendorf apparatus and perfused with Ca^{2+}-free Tyrode's solution with collagenase B & D plus protease. When the hearts became pale and flaccid they were removed from the Langendorf apparatus, the atria dissected away and sections of atrial tissue gently triturated with a Pasteur pipette to dissociate individual myocytes.

2.8 Quantitative confocal immunodetection of atrial connexins

For immunohistochemical analysis of atrial sections, hearts were quickly excised from euthanized, heparized mice (n=3 in each group). They were rinsed of blood and then either snap-frozen in liquid nitrogen or fixed in 4% formalin in PBS, embedded in paraffin and sectioned. Isolated adult atrial myocytes were fixed in 2% paraformaldehyde for 15 minutes. Atrial sections and myocytes were heated in 1X Antigen Unmasking Solution (Vector Laboratories) in a microwave oven to expose the epitope, and then blocked with 5% skim milk

in PBS for 30 minutes. Frozen sections were incubated with rabbit polyclonal anti-connexin40 (1:20, Chemicon), fixed sections with rabbit polyclonal anti-connexin43 (1:20, Zymed) and fixed myocytes were exposed to both antibodies. Sections and myocytes were rinsed in PBS, incubated with the appropriate secondary antibodies and mounted. The area of immunoreactive signal, in discrete spots from atrial sections or isolated myocytes, was quantified using single optical slices (<1μm) on the Leica TCS SP2 laser confocal system. The area of connexin immunoreactive spots and total myocardial area were quantified using the Metamorph software package (v7.2, Molecular Devices).

2.9 Western blot analysis

Protein lysates (20μg per lane) were separated using 4-12% PAGE-SDS electrophoresis and transferred onto PVDF membranes. The membranes were blocked and blotted with primary antibodies at 1:1000 against TGF-β, phospho-ERK1/2, phospho-JNK1/2, phospho-p38-MAPK, IL-1β, connexin40, connexin43, acetylated histone H3 and GAPDH. Blot densitometry was determined using NIH ImageJ software (http:/rsb.info.nih.gov), and protein band density was expressed relative to GAPDH.

2.10 Quantitative RT-PCR

Protocols for quantitative RT-PCR were performed using SYBR Green according to the manufacturer's protocol. Briefly, total RNA was isolated from whole atria of $HopX^{Tg}$ (n=4), WT (n=5) and TSA-HopX (n=5) mice. Reactions were performed in triplicate with and without RT as controls. Cycle threshold values were converted to relative gene expression levels normalized to GAPDH using the $2^{-\Delta\Delta C(t)}$ method.

2.11 Statistical analyses

Continuous variables, such as ECG intervals, cardiac conduction properties, duration of arrhythmic episodes, hemodynamic parameters, echocardiographic parameters and area of fibrosis were compared by two-way ANOVA (SPSS 12.0). Test of significance between groups was performed using Bonferroni's multiple comparisons tests. The numbers of arrhythmic episodes and animals with inducible arrhythmias were assumed to have a Poisson distribution and the Kolmogorov-Smirnov test was used to assess statistical significance between groups (SPSS 12.0). All values are reported as the mean ± standard deviation with a p-value < 0.05 considered significant.

3. Results

3.1 HDAC-inhibition reverses myocardial fibrosis

We have previously shown *HopX* over-expression induces cardiac hypertrophy with ventricular interstitial fibrosis in mice 28 weeks-old [7]. In the present study, histological analysis of the atrium and ventricle in 14-18 week-old $HopX^{Tg}$ mice reveals selective atrial interstitial fibrosis reversed to wild-type levels by trichostatin A (Fig. 1). Interestingly, development of isolated atrial fibrosis in this model is similar to findings described in the canine ventricular tachypacing-induced congestive heart failure model [8] and patients with lone AF [9].

3.2 HDAC-inhibition reduces atrial arrhythmias

Since the cardiac anatomic substrate of $HopX^{Tg}$ mice mimics that of patients and experimental models of AF with heart failure, we pursued electrophysiologic characterization to determine susceptibility for atrial arrhythmogenesis. We recorded surface ECGs from $HopX^{Tg}$ and gender-matched WT littermates that revealed p-wave duration was prolonged in $HopX^{Tg}$ compared to WT mice (25.6±1.7 ms versus 22.4 ± 1.6 ms; p=0.001; Table 1). Invasive EP

studies were performed in all mice following surface ECG analysis, and revealed $HopX^{Tg}$ mice had shorter atrial refractory periods compared to WT and TSA-WT littermates. However, the AH interval (propagation time through the atrium and atrioventricular node), HV interval (propagation time through the His bundle and bundle branches), His-bundle duration, sinus node recovery time, atrioventricular nodal and ventricular refractory periods were not different (Table 2).

Atrial programmed electrical stimulation was performed following protocols described in the Methods section of the online supplement, with the same protocol and induction attempts applied to each animal. With this protocol we induced more atrial arrhythmic episodes (48 versus 9, $p<0.001$), which were significantly longer in duration (1307 ± 289 ms versus 167 ± 114 ms, $p<0.001$) in 13 of 15 $HopX^{Tg}$ mice compared to control littermates where atrial arrhythmias were induced in only 2 of 15 WT mice and in none of the TSA-treated WT mice (Table 2 & Fig. 2B). Atrial electrical stimulation did not induce ventricular arrhythmias in any animals. Ventricular programmed electrical stimulation induced a similar number of ventricular tachycardia episodes (11 versus 10, p=NS), which were statistically no different in duration (3.31 ± 3.08 s versus 2.77 ± 1.69 s, p=NS) in 3 of 15 $HopX^{Tg}$ mice compared to 4 of 15 control mice (*P*=NS; Table 2).

Following treatment with TSA, we recorded surface ECGs from a separate cohort of $HopX^{Tg}$ (TSA-$HopX^{Tg}$) and WT (TSA-WT) mice. This analysis revealed no difference in any ECG parameters between the $HopX^{Tg}$ and TSA-$HopX^{Tg}$ mice, except p-wave duration between TSA-$HopX^{Tg}$ compared to WT (26.2 ± 2.1 ms versus 22.4 ± 1.6 ms; $p<0.001$) and TSA-WT mice (26.2 ± 2.1 ms versus 23.0 ± 1.8 ms; $p<0.05$). Invasive EP analysis of TSA-$HopX^{Tg}$ mice compared to $HopX^{Tg}$, WT or TSA-WT mice showed no difference between parameters except the atrial refractory periods, which were longer in WT and TSA-WT mice (Table 2). Interestingly, the atrial refractory periods were not different between $HopX^{Tg}$ and TSA-$HopX^{Tg}$ mice.

Atrial programmed electrical stimulation induced fewer episodes of atrial arrhythmias (5 versus 48, $p<0.01$), which were shorter in duration (148 ± 110 ms versus 1307 ± 289 ms, $p<0.01$) in 2 of 15 TSA-$HopX^{Tg}$ mice compared with 13 of 15 $HopX^{Tg}$ mice (Table 2). No atrial arrhythmias were induced in any TSA-WT mice. Similarly, ventricular programmed electrical stimulation induced fewer and shorter episodes of ventricular tachycardia in 2 of 15 TSA-$HopX^{Tg}$ mice compared to $HopX^{Tg}$ mice (*P*<0.05; Table 2).

3.3 HDAC-inhibition does not significantly alter cardiac mechanical function in $HopX^{Tg}$ mice

Evidence suggests AF may result from atrial stretch and fibrosis secondary to elevated intracardiac pressures with heart failure [10,11]. Recent studies show pressure-overload and angiotensin-induced hypertrophy are reversed by HDACi with partial normalization of ventricular function [12,13]. Therefore, we performed invasive hemodynamic studies to determine if TSA favorably effects cardiac function. We found $HopX^{Tg}$ mice have higher left ventricular end-diastolic pressure (LVEDP), reduced stroke volume and reduced cardiac output compared to WT mice (Table 3). While TSA increased cardiac output in $HopX^{Tg}$ mice, similar to its effects in mice with pressure overload ventricular hypertrophy [13], it did not affect LVEDP or myocardial relaxation with treatment initiated at 14-18 weeks of age at 0.6 mg/kg/day for 14 days (Table 3). However, heart weight to tibia length (HW/TL) and atrial weight to tibia length (AW/TL) ratios were higher in $HopX^{Tg}$ and TSA-$HopX^{Tg}$ mice compared to WT and TSA-WT, but we found no difference in HW/TL or AW/TL between $HopX^{Tg}$ compared to TSA-$HopX^{Tg}$ mice or WT compared to TSA-WT mice (Table 3).

To further characterize effects of TSA upon cardiac structure and function, we performed echocardiographic analysis. These studies revealed left atrial size is increased in $HopX^{Tg}$ mice

compared to WT littermates, however, TSA did not affect left atrial size as these were similar between $HopX^{Tg}$ compared to TSA-$HopX^{Tg}$ mice and WT compared to TSA-WT mice (Table 4, Supplement Fig. 3). In addition, the E-wave to A-wave ratio is lower in $HopX^{Tg}$ mice compared to WT mice, but not different between $HopX^{Tg}$ compared to TSA-$HopX^{Tg}$ mice; while the S-wave to D-wave ratios were not different between the four groups of mice (Table 4, Supplement Figs. 4 & 5). Further analysis reveals $HopX^{Tg}$ mice have increased ventricular wall thickness with a higher ejection fraction compared to WT littermates (Table 4). However, TSA did not affect ventricular wall thickness or ejection fraction as these were similar between $HopX^{Tg}$ and TSA-$HopX^{Tg}$ mice (Table 4). These results suggest cardiac function is reduced in $HopX^{Tg}$ compared to wild-type mice, and $HopX^{Tg}$ mice have pseudonormalization of pressures that is not affected by TSA. This must so since LVEDP and left atrial size is similar between $HopX^{Tg}$ and TSA-$HopX^{Tg}$ mice, or WT compared to TSA-WT mice and there is no evidence of mitral valve disease in this model.

3.4 Over-expressing HopX does not alter angiotensin II or downstream fibrotic pathways

Since myocardial angiotensin II is elevated with pressure- and volume-overload, and angiotensin-inhibition has favorable effects upon myocardial remodeling and AF, we sought to determine if HDACi may directly affect angiotensin. We measured myocardial angiotensin II levels in $HopX^{Tg}$ and WT mice and found no significant difference between these groups (Fig. 3A). When we assessed expression levels of TGF-β1, phospho-ERK1/2, phospho-p38-MAPK and phospho-JNK1/2 we found these were slightly lower in the atrium of $HopX^{Tg}$ compared to WT mice (Figs. 3B-E, Supplement Fig. 2A). TSA lowered expression of TGF-β1 in the atrium, which was expected since TSA inhibits TGF-β1 in the skin [14], but phospho-ERK1/2 increased with TSA compared to both WT and $HopX^{Tg}$ mice (Fig. 3). Furthermore, we found $HopX^{Tg}$ mice do have reduced atrial acetylated H3-histone, while TSA as administered in this study, augments atrial histone H3 acetylation (Fig. 3F) We also used real-time RT-PCR to assess mRNA levels of matrix metalloproteases (MMPs) and A Disintegrin and Metalloproteases (ADAMs) reported to be altered in patients with AF [15]. MMP-2, MMP-9, ADAM-10, ADAM-17 and collagen type I transcript levels were increased 2-3 fold in $HopX^{Tg}$ compared to WT mice and normalized by TSA (Supplement Table 2).

3.5 HDAC-inhibition normalizes atrial connexin40 expression and distribution

Immunohistolochemical analysis of atrial myocardium from patients with AF shows altered expression of connexins compared to myocardial sections from patients in sinus rhythm [16]. Immunoblot and immunohistochemical analysis of atrial tissue from $HopX^{Tg}$ mice revealed atrial connexin40 was significantly down-regulated compared to WT mice with no change in connexin43 expression (Fig. 4), while TSA normalized atrial connexin40 expression in $HopX^{Tg}$ mice (Figs. 4A,C).

In addition to down-regulation of atrial connexin40, we found gap junction size was altered in the atria of $HopX^{Tg}$ mice. We performed immunohistochemical analysis of connexin40 and connexin43 in isolated atrial myocytes to assess individual gap junctions without interference from those in different planes or adjacent myocytes. This analysis revealed the expression of smaller connexin40 gap junctions ($\leq 0.6\ \mu m^2$) was lower in the atrium of $HopX^{Tg}$ mice compared to that in the atria of WT mice and partially normalized in TSA-$HopX^{Tg}$ mice (Supplement Fig. 1). However, there was no difference in size distribution of atrial connexin43 gap junctions between any of the groups of mice (Supplement Fig. 1). Down-regulation of connexin40 in this setting appears to be modulated at the level of transcription, since connexin40 mRNA is reduced in the atrium of $HopX^{Tg}$ and normalized by TSA (Supplement Table 2).

4. Discussion

We have found pharmacological inhibition of HDACs reverses atrial fibrosis, normalizes atrial connexin40 expression and reduces atrial arrhythmias. While ventricular hypertrophy induced by HopX over-expression is somewhat atypical, without increased myocardial angiotensin II, this model provides useful information about the ability of HDAC inhibition to reverse the atrial substrate and arrhythmogenesis in left ventricular hypertrophy. However, these findings need to be confirmed in more typical models of pressure-overload ventricular hypertrophy. Treatment with the HDAC inhibitor trichostatin A significantly reversed the atrial arrhythmogenic substrate (i.e. reduced atrial fibrosis and normalized connexin40 expression) and rendered the atrium almost refractory to arrhythmia inducibility. These findings are particularly interesting since myocardial angiotensin II levels are unaffected in this model, suggesting HDACi has effects independent of angiotensin signaling.

4.1 Atrial structural remodeling and AF

Clinical trials [17] and animal models [5] support the contribution of angiotensin-induced atrial fibrosis in AF, and led to angiotensin-inhibition as an effective therapy for clinical AF. Still, therapeutic doses of angiotensin-inhibitors do not completely prevent atrial structural remodeling or clinical AF [5,17]. It appears angiotensin-independent mechanisms also contribute to atrial structural remodeling underlying AF [6]. Lee at al. demonstrated pirfenidone prevents atrial fibrosis and AF in a ventricular-tachypacing dog model [18]. In this model, the authors nicely showed pirfenidone inhibits TGF-β1, ERK and JNK1/2, which are all involved with the development of atrial fibrosis, but there was no investigation into the effects of pirfenidone upon angiotensin II expression or signaling in this study. Also, Millez et al. have shown atrial fibrosis and spontaneous atrial ectopy are prevented by aldactone inhibition in rats with post-infarct cardiomyopathy [11]. In this study, the authors demonstrated ACE-inhibition, beta-blockade and treatment with spironolactone reduced atrial ectopy, but only spironolactone reduced atrial fibrosis and p-wave duration that demonstrates the ability of aldactone inhibition to reverse atrial fibrosis independent of the angiotensin-renin axis. Along these lines, Burstein et al. recently showed canine atrial fibroblasts proliferate more robustly than ventricular fibroblasts in response to a variety of growth factors [19]. These investigators elegantly demonstrated atrial fibroblasts respond differently to platelet-derived growth factor, basis fibroblast growth factor, endothelin-1 and angiotensin II compared to ventricular fibroblasts, providing a rationale for why atrial-selective fibrosis occurs in some disease states and independently of angiotensin.

The results presented in this report suggest over-expressing *HopX* in the heart induces atrial-selective fibrosis, atrial connexin40 down-regulation and susceptibility for inducible atrial arrhythmias without affecting myocardial angiotensin II levels. In this setting, TSA reverses atrial fibrosis and suppresses inducible atrial arrhythmias.

4.2 Effect of HDAC-inhibition upon atrial fibrosis and arrhythmogenesis

We saw complete reversal of atrial fibrosis with low doses of TSA therapy in $HopX^{Tg}$ mice. The reduction in atrial fibrosis correlates well with reduced arrhythmogenesis in this model. Atrial interstitial fibrosis is a significant factor for driving arrhythmogenesis, supported by the fact cardiac-restricted over-expression of TGF-β1 induces selective atrial fibrosis and inducible atrial arrhythmias with no ventricular arrhythmias in transgenic mice [20]. Further support for the contribution of interstitial fibrosis to atrial arrhythmogenesis comes from the present study where we induced more episodes of atrial arrhythmias than ventricular arrhythmias and $HopX^{Tg}$ mice have increased atrial interstitial fibrosis at this age.

In considering how TSA affects interstitial fibrosis we examined TGF-β1, ERK1/2, JNK1/2 and p38-MAPK expression, which are implicated in promoting myocardial remodeling and fibrosis. We found activated TGF-β1, phospho-ERK1/2, phospho-JNK1/2 and phospho-p38-MAPK expression were lower in the atrium of $HopX^{Tg}$ compared to WT mice. While TSA reduces atrial TGF-β1, it increases phospho-ERK1/2 and phospho-JNK1/2 and had little effect upon atrial phospho-p38-MAPK. These data argue against TGF-β1, ERK1/2, JNK1/2 or p38-MAPK as the target by which TSA inhibits interstitial fibrosis in this model. Likewise, TSA increases phospho-ERK1/2 and phospho-JNK1/2 in $HopX^{Tg}$ mice and this argues against ERK1/2 or JNK1/2 modulation as a mechanism for reducing myocardial fibrosis. Still, while reductions in atrial fibrosis and arrhythmogenesis by TSA are dramatic and independent of angiotensin in this model, the exact pathways and mechanism by which these effects are induced remains to be determined.

With regards to mechanical function, TSA improves myocardial mechanical function in models of pressure-overload and angiotensin-induced hypertrophy [12,13]. Therefore, TSA may reduce atrial arrhythmogenesis by improving myocardial mechanical function and normalizing intracardiac pressures. TSA augments cardiac output in $HopX^{Tg}$ mice, probably through improvements in myocardial contractility similar to its effects in mice with pressure-overload induced ventricular hypertrophy [13]. However, while improvement in cardiac function by TSA may contribute to reduced atrial fibrosis and arrhythmogenesis, it does not appear these are mediated by normalizing left intra-atrial pressure since LVEDP remains elevated in TSA-HopXTg mice with evidence of pseudonormalization.

While TSA partially reduces cardiac hypertrophy in 3 week-old $HopX^{Tg}$ mice [7], this does not appear to be so with the older 14-18 week-old mice used in this study. This appears to be so as we saw no change in heart weight/tibial length ratio, atrial weight/tibial length ratio or left ventricular wall dimensions. In addition, the apparent discrepancy we see in the effects of HDACi upon cardiac hypertrophy in 14-18 week-old $HopX^{Tg}$ mice, compared to its effect in models of hypertrophy induced by pressure-overload or angiotensin-infusion, may be related to differences in the downstream pathways evoked by HopX over-expression. Specifically, cardiac restricted over-expression of HopX does not affect myocardial angiotensin II, and this may be a pathway HDACi affects but is not active in this model. We used a relatively low dose of TSA in this study (0.6 mg/kg/day) for a short treatment period (2 weeks) to determine if we could selectively target atrial pathology and arrhythmogenesis. This turned out to be the case in our model, and TSA at this dose and duration does augment atrial histone acetylation (Fig. 3F).

4.3 Effects of TSA upon atrial electrical remodeling and arrhythmogenesis

AF in the setting of structural heart disease is associated with altered atrial connexin expression. The expression of atrial connexin40 and connexin43 may vary based upon underlying pathology, and the only clear relationship between atrial connexins and arrhythmias appears to be heterogeneous expression [21]. However, murine models engineered with deletion of connexin40 are highly susceptible to inducible atrial arrhythmias [22]. In addition, Kanagaratnam et al. have shown that in patients with AF, atrial connexin40 expression inversely correlates with atrial conduction velocity, arrhythmia burden and complexity of the atrial activation pattern [23]. While we did not measure atrial conduction velocity or activation patterns, we did find atrial connexin40 expression is decreased in $HopX^{Tg}$ mice and normalized by TSA. Increased atrial activation time in $HopX^{Tg}$ mice, reflected as p-wave prolongation, is probably the result of increased atrial size and mass in this model since the p-wave is still prolonged in $HopX^{Tg}$ mice after treatment with TSA. Restoration of connexin40 by TSA in $HopX^{Tg}$ mice does not reduce p-wave duration, and this is not unexpected since atrial connexin40 down-regulation can increase atrial conduction velocity [24]. In addition,

decreased atrial fibrosis does not normalize p-wave duration, probably because the atria of TSA-HopX^{Tg} mice are still enlarged and similar in mass to that of HopX^{Tg} mice. The combined effects of increased interstitial fibrosis and down-regulation of atrial connexin40 probably contribute to the electrical uncoupling and non-uniformities in conduction between myocytes that promotes atrial arrhythmogenesis.

4.4 Novel aspects and potential significance

To the best of our knowledge, this is the first study demonstrating the efficacy of HDAC inhibition to reverse atrial fibrosis and arrhythmogenesis independent of the renin-angiotensin cascade. This is important because angiotensin-inhibition, while effective for preventing atrial structural remodeling and reducing AF, only partially inhibits atrial fibrosis with a significant burden of AF untreated. Our findings indicate TSA reverses atrial fibrosis and arrhythmia inducibility, with normalization of atrial connexin40 expression in this model of left ventricular hypertrophy. These anti-arrhythmic effects of TSA appear to be independent of angiotensin II expression, TGF-β1, ERK1/2, changes in atrial refractoriness or alterations in intracardiac pressures.

Supplementary Material

Refer to Web version on PubMed Central for supplementary material.

Acknowledgements

Sources of funding This work was supported by grants from the National Heart, Lung Blood Institute, National Institutes of Health (VVP, JAE), the McCabe Foundation (VVP), the Barra Foundation (VVP), and a National Institutes of Health Institutional Career Research Award to the Children's Hospital of Philadelphia (MDL).

References

1. Tsang TS, Gersh BJ, Appleton CP, Tajik AJ, Barnes ME, Bailey KR, et al. Left ventricular diastolic dysfunction as a predictor of the first diagnosed nonvalvular atrial fibrillation in 840 elderly men and women. J Am Coll Cardiol 2002;40:1636–44. [PubMed: 12427417]
2. Okin PM, Wachtell K, Devereux RB, Harris KE, Jern S, Kjeldsen SE, et al. Regression of electrocardiographic left ventricular hypertrophy and decreased incidence of new-onset Atrial fibrillation in patients with hypertension. JAMA 2006;296:1242–8. [PubMed: 16968848]
3. Rotter M, Jais P, Garrigue S, Sanders P, Hocini M, Hsu L-F, et al. Clinical predictors of noninducibility of sustained atrial fibrillation after pulmonary vein isolation. J Cardiovas Electrophysiol 2005;16:1298–303.
4. Li D, Fareh S, Leung TK, Nattel S. Promotion of atrial fibrillation by heart failure in dogs: atrial remodeling of a different sort. Circulation 1999;100:87–95. [PubMed: 10393686]
5. Li D, Shinagawa K, Pang L, Leung TK, Cardin S, Wang Z, et al. Effects of angiotensin-converting enzyme inhibition on the development of the atrial fibrillation substrate in dogs with ventricular tachypacing-induced congestive heart failure. Circulation 2001;104:2608–14. [PubMed: 11714658]
6. Cardin S, Li D, Thorin-Trescases N, Leung T-K, Thorin E, Nattel S. Evolution of the atrial fibrillation substrate in experimental congestive heart failure: angiotensin-dependent and -independent pathways. Cardiovasc Res 2003;60:315–25. [PubMed: 14613861]
7. Kook H, Lepore JJ, Gitler AD, Lu MM, Wing-Man Yung W, Mackay J, et al. Cardiac hypertrophy and histone deacetylase-dependent transcriptional repression mediated by the atypical homeodomain protein Hop. J Clin Invest 2003;112:863–71. [PubMed: 12975471]
8. Hanna N, Cardin S, Leung T-K, Nattel S. Differences in atrial versus ventricular remodeling in dogs with ventricular tachypacing-induced congestive heart failure. Cardiovasc Res 2004;63:236–44. [PubMed: 15249181]
9. Frustaci A, Chimenti C, Bellocci F, Morgante E, Russo MA, Maseri A. Histological substrate of atrial biopsies in patients with lone atrial fibrillation. Circulation 1997;96:1180–4. [PubMed: 9286947]

10. Schoonderwoerd BA, Van Gelder IC, Van Veldhuisen DJ, Van den Berg MP, Crijns HJGM. Electrical and structural remodeling: role in the genesis and maintenance of atrial fibrillation. Prog Cardiovasc Dis 2005;48:153–68. [PubMed: 16271942]
11. Milliez P, DeAngelis N, Rucker-Martin C, Leenhardt A, Vicaut E, Robidel E, et al. Spironolactone reduces fibrosis of dilated atria during heart failure in rats with myocardial infarction. Eur Heart J 2005;26:2193–9. [PubMed: 16141258]
12. Kee HJ, Sohn IS, Nam KI, Park JE, Qian YR, Yin Z, et al. Inhibition of histone deacetylation blocks cardiac hypertrophy induced by angiotensin II infusion and aortic banding. Circulation 2006;113:51–9. [PubMed: 16380549]
13. Kong Y, Tannous P, Lu G, Berenji K, Rothermel BA, Olson EN, et al. Suppression of class I and II histone deacetylases blunts pressure-overload cardiac hypertrophy. Circulation 2006;113:2579–88. [PubMed: 16735673]
14. Rombouts K, Niki T, Greenwel P, Vandermonde A, Wielant A, Hellemans K, et al. Trichostatin A, a histone deacetylase inhibitor, suppresses collagen synthesis and prevents TGF-ß1-induced fibrogenesis in skin fibroblasts. Experimental Cell Research 2002;278:184–97. [PubMed: 12169274]
15. Arndt M, Lendeckel U, Rocken C, Nepple K, Wolke C, Spiess A, et al. Altered expression of ADAMs (A Disintegrin And Metalloproteinase) in fibrillating human atria. Circulation 2002;105:720–5. [PubMed: 11839628]
16. Polontchouk L, Haefliger J-A, Ebelt B, Schaefer T, Stuhlmann D, Mehlhorn U, et al. Effects of chronic atrial fibrillation on gap junction distribution in human and rat atria. J Am Coll Cardiol 2001;38:883–91. [PubMed: 11527649]
17. Vermes E, Tardif J-C, Bourassa MG, Racine N, Levesque S, White M, et al. Enalapril decreases the incidence of atrial fibrillation in patients with left ventricular dysfunction: insight from the studies of left ventricular dysfunction (SOLVD) trials. Circulation 2003;107:2926–31. [PubMed: 12771010]
18. Lee KW, Everett THIV, Rahmutula D, Guerra JM, Wilson E, Ding C, et al. Pirfenidone prevents the development of a vulnerable substrate for atrial fibrillation in a canine model of heart failure. Circulation 2006;114:1703–12. [PubMed: 17030685]
19. Burstein B, Libby E, Calderone A, Nattel S. Differential behaviors of atrial versus ventricular fibroblasts: a potential role for platelet-derived growth factor in atrial-ventricular remodeling differences. Circulation 2008;117:1630–41. [PubMed: 18347210]
20. Verheule S, Sato T, Everett T IV, Engle SK, Otten D, Rubart-von der Lohe M, et al. Increased vulnerability to atrial fibrillation in transgenic mice with selective atrial fibrosis caused by overexpression of TGF-ß1. Circ Res 2004;94:1458–65. [PubMed: 15117823]
21. Nattel S, Maguy A, Le Bouter S, Yeh Y-H. Arrhythmogenic ion-channel remodeling in the heart: heart failure, myocardial infarction and atrial fibrillation. Physiol Rev 2007;87:425–56. [PubMed: 17429037]
22. Hagendorff A, Schumacher B, Kirchhoff S, Lüderitz B, Willecke K. Conduction disturbances and increased atrial vulnerability in Connexin40-deficient mice analyzed by transesophageal stimulation. Circulation 1999;99:1508–15. [PubMed: 10086977]
23. Kanagaratnam P, Cherian A, Stanbridge RDL, Glenville B, Severs NJ, Peters NS. Relationship between connexins and atrial activation during human atrial fibrillation. J of Cardiovas Electrophysiol 2004;15:206–16.
24. Beauchamp P, Yamada KA, Baertschi AJ, Green K, Kanter EM, Saffitz JE, et al. Relative contributions of connexins 40 and 43 to atrial impulse propagation in synthetic strands of neonatal and fetal murine cardiomyocytes. Circ Res 2006;99:1216–24. [PubMed: 17053190]

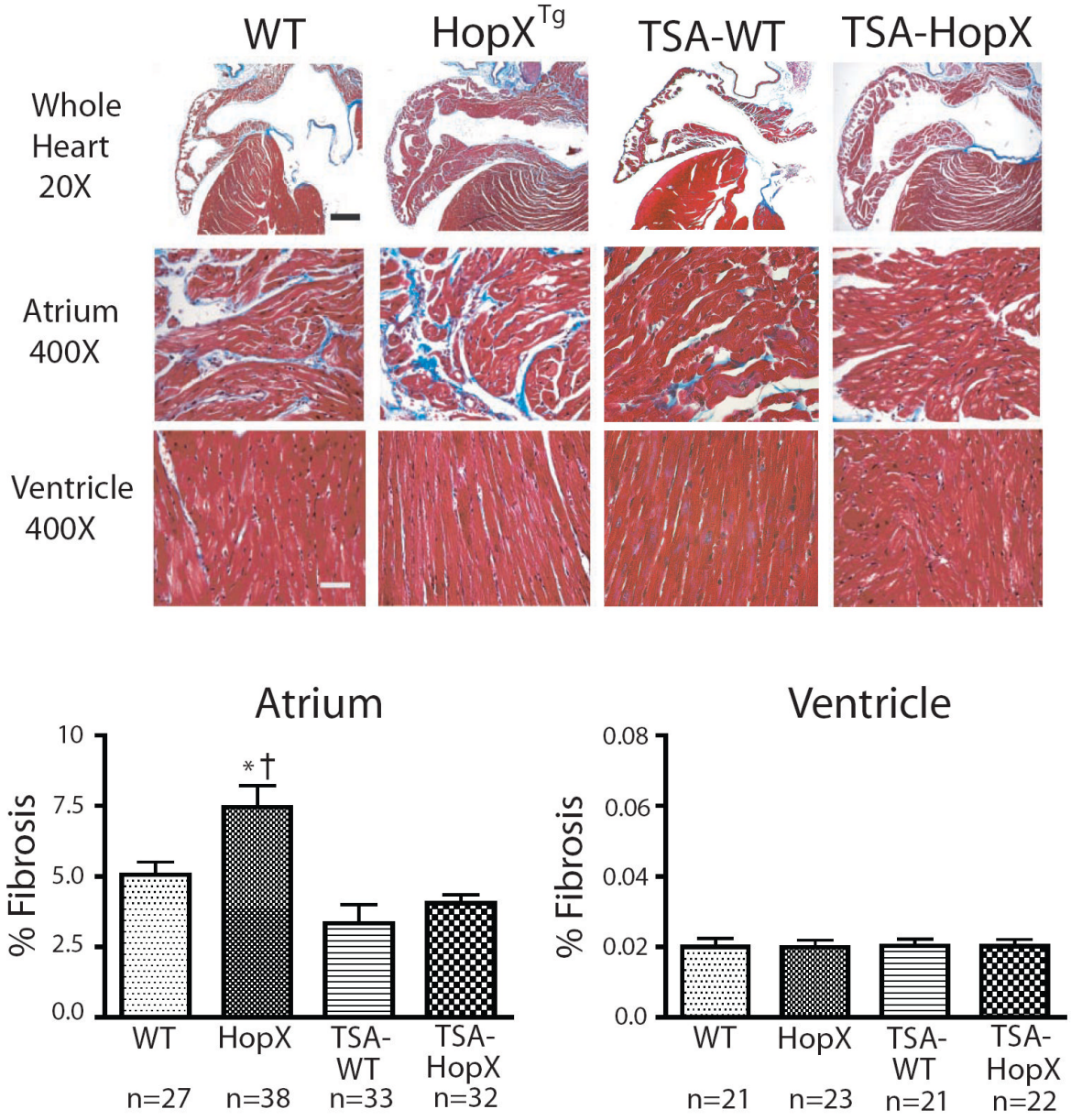

Fig. 1.

Atrial fibrosis is reversed by trichostatin A. Masson's trichrome staining reveals increased atrial interstitial fibrosis in HopX transgenic mice ($HopX^{Tg}$) compared with wild-type controls (WT), while treatment with trichostatin A (TSA-HopX) resulted in complete reversal of atrial fibrosis. Note there is no obvious ventricular interstitial fibrosis in the four groups shown. Scale Bar: 40X images = 1 mm; 400X images = 100 μm. Percentage of interstitial fibrosis. There was a significant increase in atrial fibrosis (left panel) in the $HopX^{Tg}$ group compared with wild-type controls, while treatment with TSA resulted in a significant reduction of atrial fibrosis. There was no significant ventricular fibrosis (right panel) detected in any the groups examined. *$p<0.01$ compared to WT; $^{\dagger}p<0.01$ compared to $HopX^{Tg}$; $^{\S}p<0.01$ compared to TSA-WT.

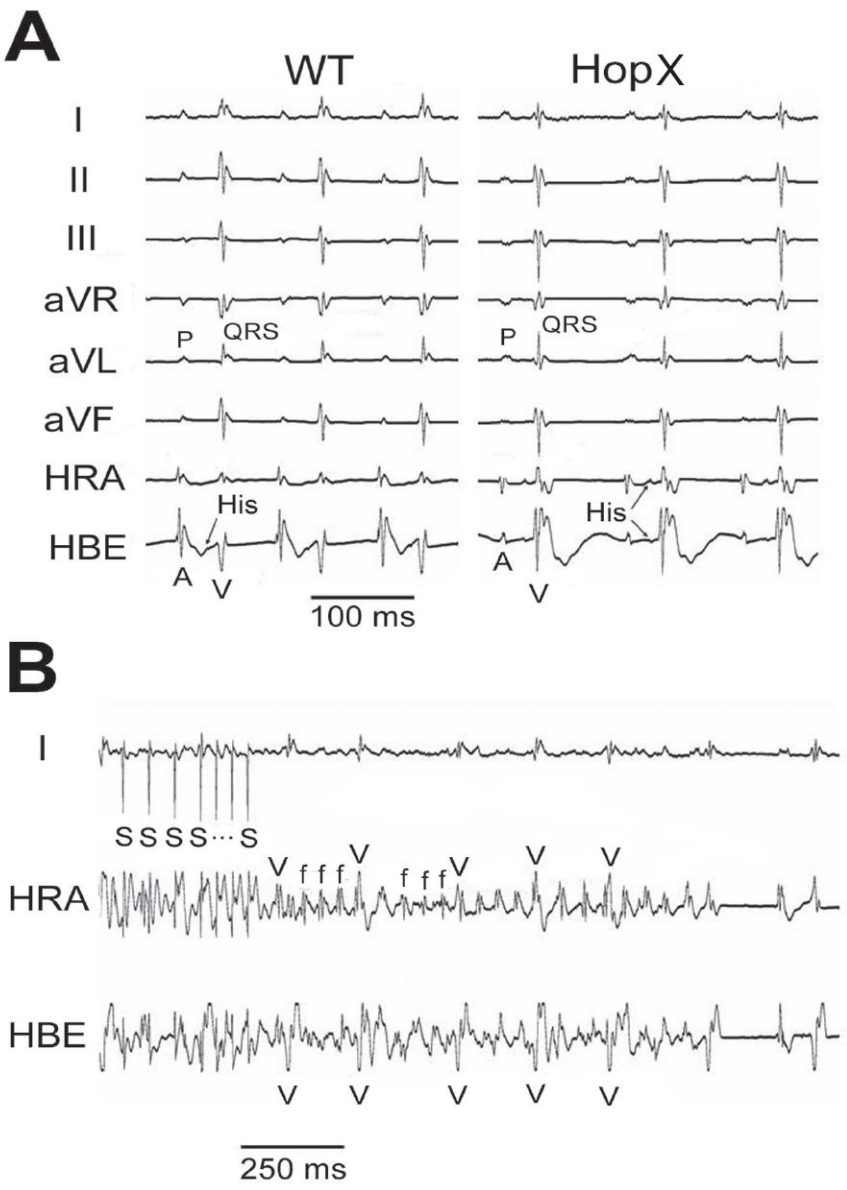

Fig. 2.

Atrial arrhythmias induced in HopX transgenic mice. (A) Representative surface electrocardiograms from a HopX transgenic (TG) and wild-type (WT) littermate mouse demonstrating normal electrocardiographic morphologies in both animals. (B) Shown are recordings from lead I (I), the high right atrium (HRA) and the right ventricular apex (RVA) demonstrating a run of atrial fibrillation induced by burst stimulation (S) in a HopX transgenic mouse. Irregularly irregular intervals between ventricular (V) beats can be seen on both the intracardiac leads and surface lead. Sinus beats are shown upon termination of the episode with normal atrial (a) and ventricular (v) intracardiac electrograms.

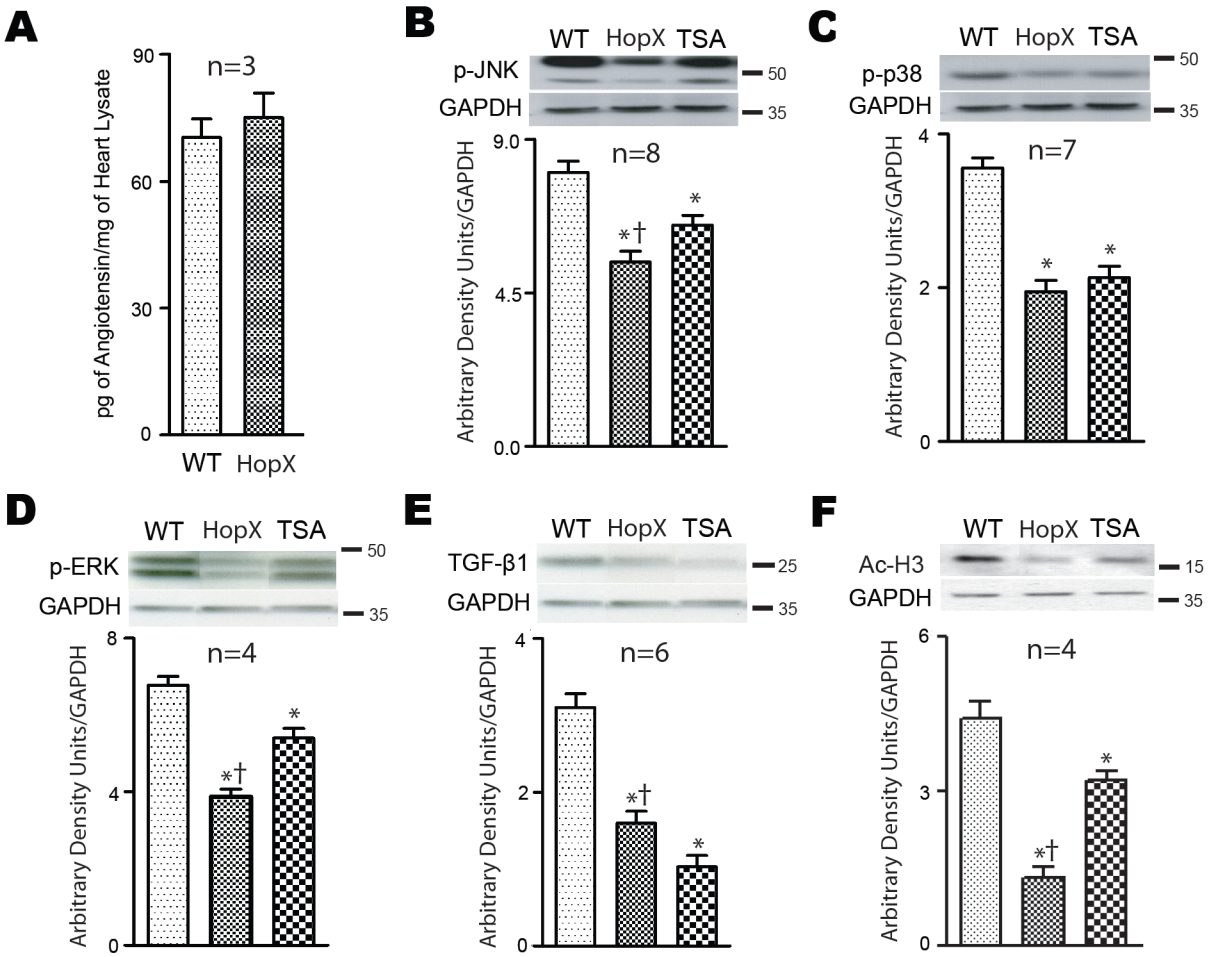

Fig. 3.

Atrial angiotensin and cytokines are not elevated by HopX. (A) ELISA shows no difference in angiotensin II levels in WT and HopX^{Tg} hearts. Immunoblots shows atrial levels of (B) phospho-JNK1/2 (46- and 54-kDa isoforms), (C) phospho-p38-MAPK (42-kDa), (D) phospho-ERK1/2 (42- and 44-kDa isoforms), (E) active TGF-β1 (25-kDa) and (F) acetylated histone H3 (Ac-H3, 17-kDa). Below the blots are band signal intensities normalized to GAPDH (both isoforms of ERK and JNK1/2 were averaged together for quantitative analysis). Active TGF-β1 is lower in HopX^{Tg} mice relative to control and further decreased in TSA-HopX^{Tg} mice. Phospho-ERK1/2 is also lower in HopX^{Tg} mice relative to control but increased in TSA-HopX^{Tg} mice. Phospho-JNK1/2 and phospho-p38-MAPK were not different between HopX^{Tg}, TSA-HopX^{Tg} or control mice. *P<0.05 compared to WT; †P<0.05 compared to TSA-HopX^{Tg}.

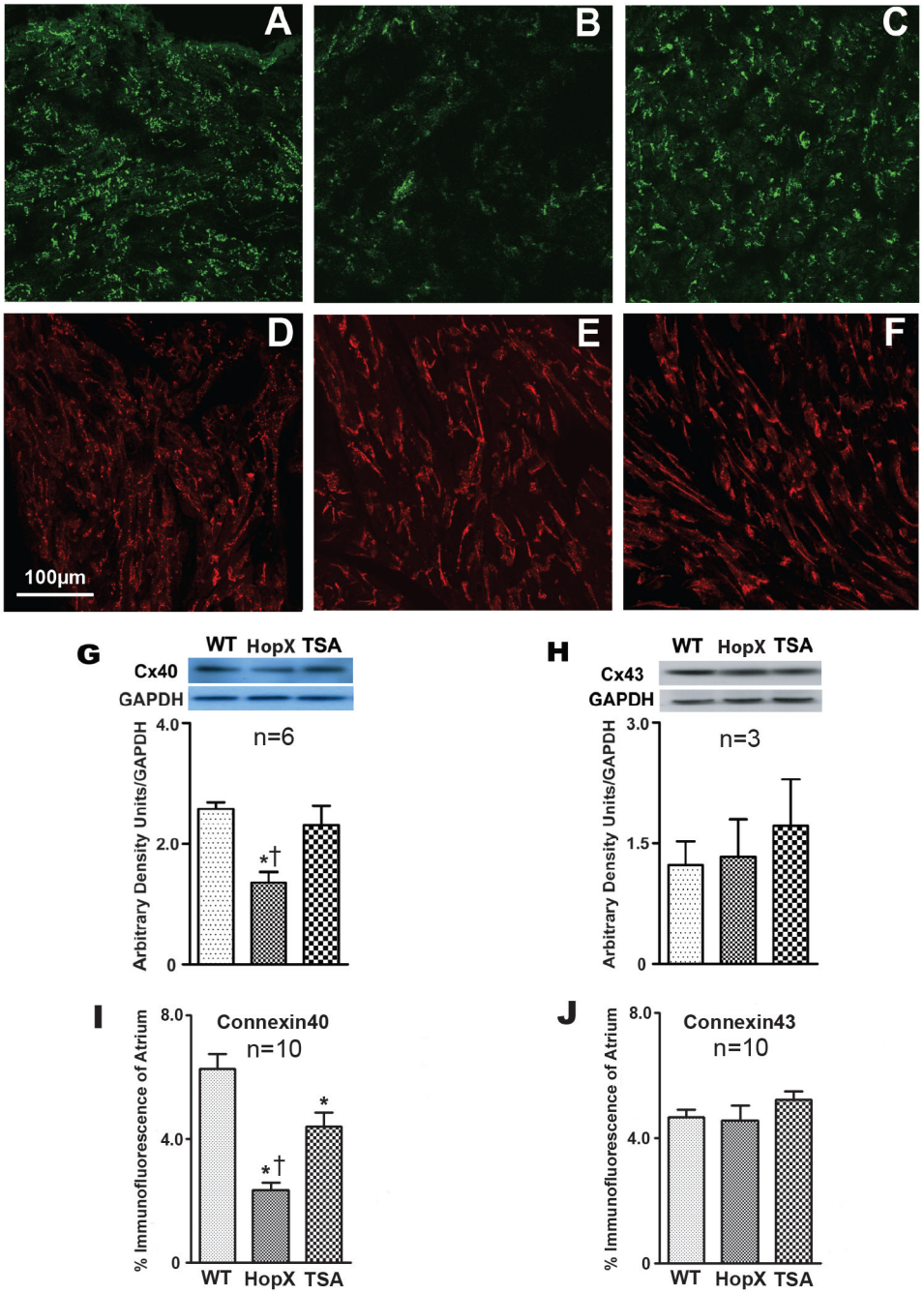

Fig. 4.

Atrial connexin40 expression is reduced in left ventricular hypertrophy and normalized by trichostatin A. Shown is staining for connexin40 in (A) WT, (B) $HopX^{Tg}$ and (C) TSA-$HopX^{Tg}$ mice and for connexin43 in (D) WT, (E) $HopX^{Tg}$ and (F) TSA- $HopX^{Tg}$ mice. Scale bar = 100 μm. Panel (G) shows immunoblot analysis of atrial connexin40 that is lower in $HopX^{Tg}$ mice and normalized by TSA, while panel (H) show the same analysis for connexin43 that is not affected by HopX or TSA. Blots are representative of three separate experiments. Panel (I) shows the normalized size distribution of connexin40 gap junctions with the same analysis of connexin43 gap junctions in panel (J). The expression of total connexin40 gap is lower in the atrium $HopX^{Tg}$ mice and almost completely normalized by TSA Data averaged

from 10 different sections using 3 separate atria in each group. *P<0.05 compared to WT; †P<0.05 compared to TSA-HopX^{Tg}.

Table 1

Surface ECG parameters in HopX transgenic mice.

	HopX^{Tg} (n=15)	**WT (n=15)**	**TSA-HopX^{Tg} (n=15)**	**TSA-WT (n=10)**
SCL (ms)	163 ± 36.3	155 ± 27.4	158 ± 32.6	160 ± 29.3
HR (bpm)	368 ± 84.6	388 ± 63.5	380 ± 72.3	370 ± 64.8
P-wave (ms)	25.6 ± 1.7	22.4 ± 1.6*†	26.2 ± 2.1	23.0 ± 1.8
PR (ms)	44.2 ± 7.3	43.0 ± 6.4	42.1 ± 7.2	43.7 ± 6/0
QRS (ms)	10.4 ± 1.6	10.3 ± 1.8	10.8 ± 1.5	10.0 ± 1.2
QT (ms)	20.7 ± 2.9	21.5 ± 2.1	21.0 ± 2.3	21.8 ± 2.7
QTm (ms)	16.4 ± 2.4	17.5 ± 2.2	17.0 ± 2.2	17.9 ± 2.0
Age (d)	108.5 ± 6.4†§	109.2 ± 7.2†§	121.5 ± 8.0	119.8 ± 7.6
Weight (g)	31.0 ± 5.2	31.7 ± 5.3	29.7 ± 4.1	28.4. ± 3.5

*P<0.05 compared to WT;

†P<0.05 compared to TSA-HopX^{Tg};

§P<0.05 compared to TSA-WT.

SCL = Sinus cycle length; HR = Heart rate; P-wave = P-wave duration; PR = PR-interval duration; QRS = QRS-complex width; QT = QT-interval duration; QT_m = Corrected QT-interval duration.

Table 2

Invasive EP parameters in HopX transgenic mice.

	HopX^{Tg} (n=15)	**WT (n=15)**	**TSA-HopX^{Tg} (n=15)**	**TSA-WT (n=10)**
SCL (ms)	168 ± 52.5	157 ± 28.7	158 ± 20.7	160 ± 30.7
HR (bpm)	357 ± 112	382 ± 69.8	380 ± 81.9	370 ± 59.4
AH (ms)	30.6 ± 2.5	32.4 ± 4.2	29.6 ± 3.3	31.3 ± 3.8
H_d (ms)	5.1 ± 1.1	5.3 ± 1.1	4.5 ± 1.0	4.9 ± 0.9
HV (ms)	14.4 ± 2.7	13.7 ± 1.7	12.8 ± 1.8	12.6 ± 1.9
AVI (ms)	46.1 ± 5.6	45.9 ± 4.3	43.9 ± 4.3	44.8 ± 4.5
$SNRT_{120}$ (ms)	235 ± 106	224 ± 72.0	228 ± 96.9	230 ± 86.2
$SNRT_{100}$ (ms)	231 ± 96.5	222 ± 72.4	236 ± 86.5	233 ± 79.8
$AVERP_{120}$ (ms)	83.6 ± 14.6	86.5 ± 7.8	79.5 ± 14.4	88.1 ± 10.4
AVNWBCL (ms)	114 ± 17.9	111 ± 9.6	104 ± 18.1	107 ± 11.2
$AERP_{120}$ (ms)	37.5 ± 9.2*§	46.7 ± 7.8	35.5 ± 7.9*§	44.8 ± 4.6*
$AERP_{100}$ (ms)	37.0 ± 9.5*§	45.8 ± 6.7	35.0 ± 7.1*§	44.5 ± 5.0*
$VERP_{120}$ (ms)	44.0 ± 9.7	45.8 ± 12.4	40.4 ± 9.8	44.7 ± 8.4
$VERP_{100}$ (ms)	47.0 ± 8.2	47.9 ± 10.3	41.8 ± 9.4	44.5 ± 8.8
Episodes AT	48*†§	9	5	0
Duration AT (s)	1.307 ± 0.289*†	0.167 ± 0.114	0.148 ± 0.110	-
AT CL (ms)	46.2 ± 10.0	45.4 ± 5.5	47.0 ± 7.2	-
Mice with AT	13/15*†	2/15	2/15	-
Episodes VT	11†§	10†§	4	5
Duration VT (s)	3.31 ± 3.08	2.77 ± 1.69	0.89 ± 1.07	1.32 ± 1.14
VT CL (ms)	50.7 ± 9.9	51.5 ± 7.8	50.4 ± 8.6	51.6 ± 9.4
Mice with VT	3/15	4/15	2/15	2/10

*P<0.05 compared to WT;

†P<0.05 compared to TSA-HopX^{Tg};

§P<0.05 compared to TSA-WT.

AH = AtrioHisian interval; Hd = His-duration; HV= Hisioventricular interval; AVI = Atrioventricular interval; $SNRT_{120}$ = Sinus node recovery time at drive train of 120 ms; $SNRT_{100}$ = Sinus node recovery time at drive train of 100 ms; $AERP_{120}$ = Atrial ERP at drive train of 120 ms; $AERP_{100}$ = Atrial ERP at drive train of 100 ms; $AVERP_{120}$ = Atrioventricular ERP, drive train 120 ms; AVWBCL = AV Wenckebach block cycle length; AV 2:1 = AV 2:1 block cycle length; VAWBCL = Ventriculoatrial Wenckebach block cycle length; $VERP_{120}$ = Ventricular ERP at drive train of 120 ms; $VERP_{100}$ = Ventricular ERP at drive train of 100 ms.

Table 3

Invasive hemodynamic and morphometric parameters in HopX transgenic mice.

	HopX^{Tg} (n=7)	**WT (n=7)**	**TSA-HopX^{Tg} (n=7)**	**TSA-WT (n=7)**
Heart rate (bpm)	388 ± 58.4	405 ± 51.0	397 ± 60.1	412 ± 60.6
LV end systolic pressure (mmHg)	98.7 ± 11.8	104 ± 10.6	102 ± 9.2	101 ± 9.7
LV end diastolic pressure (mmHg)	8.7 ± 1.9 *§	4.2 ± 1.7	9.0 ± 2.3 *§	3.9 ± 2.0
Cardiac output (μl/min)	7115 ± 1134 *†§	8695 ± 1202	8263 ± 1041	9054 ± 1065
Positive dP/dt (mmHg/s)	10982 ± 2778	12837 ± 3005	11352 ± 2631	12830 ± 2658
Negative dP/dt (mmHg/s)	-6385 ± 1687	-7457 ± 1824	-6248 ± 1589	-7645 ± 1453
Stroke volume (μl)	18.3 ± 2.9	21.5 ± 3.0	20.8 ± 2.6	22.0 ± 2.7
Tau – Weiss (ms)	7.86 ± 1.5	7.25 ± 2.0	8.36 ± 2.2	8.10 ± 1.7
Tau – Glantz (ms)	16.5 ± 2.9 *§	9.74 ± 1.4	15.0 ± 2.5 *§	11.0 ± 2.0
	HopX^{Tg} (n=11)	WT (n=15)	TSA-HopX^{Tg} (n=13)	TSA-WT (n=10)
Heart weight (mg)	201 ± 17.0 *§	121.4 ± 11.5	192.8 ± 15.5 *§	128.2 ± 12.2
Heart weight/body weight (mg/g)	11.0 ± 1.0 *§	8.1 ± 0.83	10.4 ± 0.72 *§	7.7 ± 0.67
Heart weight/tibia length (mg/mm)	10.2 ± 0.15 *§	7.4 ± 1.4	10.5 ± 0.86 *§	7.0 ± 0.53
	HopX^{Tg} (n=12)	WT (n=13)	TSA-HopX^{Tg} (n=9)	TSA-WT (n=10)
Atrial weight (mg)	24 ± 2.5 *§	13.95 ± 1.86	23.4 ± 2.9 *§	13.3 ± 1.7
Atrial weight/body weight (mg/g)	0.86 ± 0.13 *§	0.50 ± 0.07	0.90 ± 0.11 *§	0.43 ± 0.15
Atrial weight/tibia length (mg/mm)	1.42 ± 0.28 *§	0.78 ± 0.09	1.3 ± 0.17 *§	0.73 ± 0.19

*P<0.05 compared to WT;

†P<0.05 compared to TSA-HopX^{Tg};

§P<0.05 compared to TSA-WT.

LV=left ventricular.

Table 4

Echocardiographic parameters in HopX transgenic mice.

	HopX^{Tg} (n=7)	WT (n=7)	TSA-HopX^{Tg} (n=7)	TSA-WT (n=7)
Left Ventricle Posterior Wall (mm)	1.19 ± 0.22*§	0.71 ± 0.06	1.11 ± 0.13*§	0.72 ± 0.08
Intra-ventricle Septum (mm)	1.22 ± 0.25*§	0.74 ± 0.05	1.15 ± 0.16*§	0.68 ± 0.10
LV Fractional Shortening (%)	55.0 ± 13.4*§	32.8 ± 3.50	51.7 ± 5.34*§	34.2 ± 2.08
LV Ejection Fraction (%)	84.3 ± 11.1*§	61.5 ± 4.71	84.2 ± 6.65*§	63.9 ± 2.66
LA End-Diastolic Long Axis (mm)	2.32 ± 0.48	1.59 ± 0.21	2.15 ± 0.19	1.85 ± 0.16
LA End-Diastolic Short Axis (mm)	2.50 ± 0.39	1.87 ± 0.20	2.45 ± 0.29	1.93 ± 0.20
E-to-A Wave Ratio	1.14 ± 0.05*§	1.38 ± 0.07	1.00 ± 0.11*§	1.41 ± 0.20
S-to-D Wave Ratio	0.42 ± 0.12	0.57 ± 0.20	0.56 ± 0.10	0.47 ± 0.06

*P<0.05 compared to WT;

†P<0.05 compared to TSA-HopX^{Tg};

§P<0.05 compared to TSA-WT.

LV=left ventricular; LA=left atrial.